ELSEVIER

Biochimica et Biophysica Acta 1240 (1995) 133–141

BBA Biochimica et Biophysica Acta

Structure and properties of *N*-palmitoleoylgalactosylsphingosine (cerebroside)

Nelson S. Haas, G. Graham Shipley *

Departments of Biophysics and Biochemistry, Boston University School of Medicine, Center for Advanced Biomedical Research, 80 East Concord Street, Boston, MA 02118-2394, USA

Received 17 February 1995; revised 2 June 1995; accepted 10 July 1995

Abstract

Differential scanning calorimetry (DSC) and X-ray diffraction have been used to study the structure and properties of *N*-palmitoleoylgalactosylsphingosine (NPoGS; 16:1 galactocerebroside). DSC of fully hydrated NPoGS shows a complex pattern of three endothermic transitions at 35, 39 and 53°C. Using a combination of thermal protocols (varying heating/cooling rates, incubation at different temperatures, etc.), the three ordered chain (gel) phases responsible for the transitions have been isolated; transition I ($T_m = 35$°C; $\Delta H_I = 6.3$ kcal/mol), transition II ($T_m = 39$°C; $\Delta H_{II} = 8.6$ kcal/mol), and transition III ($T_m = 53$°C; $\Delta H_{III} = 12.8$ kcal/mol). The gel phases do not interconvert but rather form independently following cooling from the melted chain phase. X-ray diffraction data of the three isolated phases confirm that they all are bilayer structures with different bilayer periodicities (L_I, 50.7 Å; L_{II}, 51.7 Å; $L_{III} = 49.2$ Å) and different chain packing modes. The L_I, L_{II}, and L_{III} bilayer phases each melt independently to the melted chain L_α phase. Comparisons with other cerebrosides make it clear that alterations in chain length and chain unsaturation markedly affect the thermotropic behavior of cerebrosides and the metastable and stable phases they are able to form. As with phospholipids, introduction of *cis*-unsaturation into the *N*-acyl chain reduces both the chain melting temperature and enthalpy.

Keywords: Cerebroside; DSC; X-ray diffraction; Bilayer; Membrane

1. Introduction

Glycosphingolipids, most notably cerebrosides and gangliosides, are present in the plasma membranes of most mammalian cells. They exhibit marked asymmetry in their location, which appears to be exclusively in the membrane bilayer outer leaflet. In most cases glycosphingolipids are present in relatively small amounts, although some tissues in higher animals, such as the central and peripheral nervous system, contain relatively large amounts. Cerebrosides, particularly galactocerebrosides, are a major lipid constituent of peripheral nerve myelin [1,2].

The structure and properties of cerebrosides have been studied by a variety of methods, including: spectroscopy [3–6], scanning calorimetry [7–15], surface monolayers [16–18], and X-ray diffraction [13–15,19–22]. Single-crystal X-ray diffraction studies of a synthetic galactosyl cerebroside show a bilayer packing arrangement with the galactosyl head groups aligned nearly parallel to the plane of the bilayer [23]. An extensive system of polar and hydrogen-bonding groups allows for a strong network of intermolecular interactions. Contributing to the hydrogen-bonding network are hydroxyl (including those in the sugar head groups), carbonyl, and amide groups [23].

When considering membrane lipid behavior, one important issue is the effect of chain unsaturation. This has been studied most extensively with membrane phospholipids such as phosphatidylcholine and phosphatidylethanolamine. For example, Coolbear et al. [24] showed that a single *cis* double bond (Δ9-10) introduced into 18 carbon (C_{18}) phosphatidylcholines in the *sn*-2 fatty acid decreased the chain melting temperature by about 50°C. A second *cis* double bond (18:2; Δ9-10, 12-13) caused a further 12°C reduction, however, a third *cis* double bond (18:3; Δ9-10,

Abbreviations: DSC, differential scanning calorimetry; NPoGS, *N*-palmitoleoylgalactosylsphingosine (cerebroside).

* Corresponding author. Tel: +1 (617) 6384009; fax: +1 (617) 6384041; e-mail: shipley@med-biophi.bu.edu.

SSDI 0005-2736(95)00174-3

12-13, 15-16) had little additional effect on chain melting. Thus, introduction of the first *cis* double bond apparently causes the greatest perturbation in the bilayer structure.

Our laboratory has made a systematic study of the effects of varying chain length and unsaturation on the structure and properties of galactosyl cerebrosides. In the past, studies of the 16:0-, 18:0-, and 24:0-galactosyl cerebrosides [13–15], and the 18:0-, 18:1 (*cis* Δ9-10)-, and 18:2 (*cis* Δ9-10, 12-13)-cerebrosides [15] have revealed some of the effects of chain length and *cis* unsaturation on this important class of lipids. While chain-unsaturation again produces a marked reduction in the chain-melting temperature, interesting alterations in the low temperature gel and crystalline phases are observed [15]. To explore further these issues, we report here a study of the galactosyl cerebroside with an *N*-linked, 16-carbon, *cis* Δ9-10-monounsaturated (16:1) fatty acid, *N*-palmitoleoylgalactosylsphingosine, NPoGS. Particular attention is paid to the complex thermotropic behavior of NPoGS and the structures of the different ordered-chain phases formed, rather than the molecular conformation of NPoGS in the different phases. Comparison with the behavior of other galactosyl cerebrosides permits general conclusions to be drawn about the influence of chain length and/or unsaturation on cerebroside properties.

2. Materials and methods

2.1. Samples

NPoGS was kindly provided by Skarjune and Oldfield, who synthesized NPoGS according to their own method [4,25] using pig brain cerebroside, based on the isolation, deacylation, and reacylation techniques of Radin [26–28]. It is estimated that NPoGS contains mainly 18:1 *trans* sphingosine with approximately 5% of the dihydrosphingosine derivative. Lipid purity was checked by silica-gel thin-layer chromatography with the solvent system chloroform/methanol/water (65:25:4, v/v), which yielded a single spot after sulfuric acid charring.

2.2. Differential scanning calorimetry (DSC)

Milligram quantities of NPoGS were weighed into stainless steel DSC pans and gravimetrically hydrated to 70 wt% H_2O with doubly-distilled water. The pans were hermetically sealed and repeatedly cycled between −10°C and 70°C to ensure equilibration. DSC studies were performed on a Perkin-Elmer (Norwalk, CT) DSC-2 linked to a Thermal Analysis Data Station (TADS). TADS analyses yielded transition peak temperatures (T) and transition enthalpies (ΔH); transition entropies (ΔS) were computed from T and ΔH. Calibration was made using the standards gallium and dipalmitoylphosphatidylcholine.

Prior to a DSC procedure or the start of an incubation, NPoGS was heated above its highest transition, to 70°C and cooled to −10°C. Various heating and cooling procedures were used to determine the thermodynamic and kinetic properties of NPoGS. These procedures included: varying heating and cooling scan rates between 0.3125 C°/min and 40 C°/min; varying pre-scan cooling rates between 0.3125 C°/min and 40 C°/min; incubating at −10°C, −12°C, 38°C, and 45°C for various times; and heating to temperatures other than 70°C with subsequent heating and/or cooling scans.

2.3. X-ray diffraction

The X-ray diffraction experiments were conducted with copper K_α radiation ($\lambda = 1.5418$ Å) from either an Elliot GX-6 rotating anode generator (Elliot Automation, Borehamwood, UK) using toroidal optics, exposure time 4–6 h [29], or an Elliot GX-20 rotating anode generator using double-mirror optics, exposure time 24–48 h [30]. X-ray diffraction patterns were recorded on photographic film and diffraction intensities recorded using a scanning microdensitometer (Joyce-Loebl, Gateshead, UK).

X-ray samples, hydrated to 70 wt% water, were prepared by weighing NPoGS and doubly-distilled water into 1 mm diameter, thin-walled, glass capillary tubes. The contents of the tubes were centrifuged to the bottom of the tubes, and the tops of the tubes were flame-sealed. After sealing, the tube contents were repeatedly centrifuged, at 70°C, between the ends of the capillary to ensure equilibration. Samples were heated to 70°C and centrifuged before recording X-ray diffraction data. To obtain single phases for NPoGS, the X-ray samples were heated and cooled according to DSC protocols which yielded single DSC peaks. Strict control of heating and cooling rates was accomplished via a manually controlled water bath; the sample temperature was maintained (±1 C°) with an automatically controlled ethylene glycol/water circulating bath.

3. Results

3.1. Differential scanning calorimetry

The reversible DSC behavior of fully hydrated (70% H_2O) NPoGS is illustrated in Fig. 1. Fig. 1a shows an initial heating scan following cooling from 70°C at 5 C°/min. This scan shows that NPoGS, heated at 5 C°/min, undergoes a complex endothermic transition with maxima at 35°C and 39°C, followed by a high temperature endothermic transition at 53°C. Cooling at 5 C°/min to −10°C (Fig. 1b) shows an exothermic transition at 10°C with a high temperature shoulder at ~15°C. Immediate reheating (Fig. 1c) produces behavior identical to that

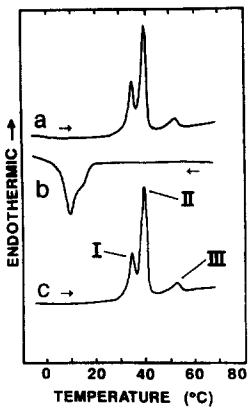

Fig. 1. DSC behavior of NPoGS at heating/cooling rates of 5 C°/min: (a) Initial heating scan immediately following cooling from 70°C at 5 C°/min. (b) Immediate cooling scan and (c) Immediate reheating scan.

shown in Fig. 1a. This DSC behavior suggests the presence of three low temperature phases, giving rise to the three transitions labeled I, II, and III (see Fig. 1c). To isolate the phases responsible for the three transitions, the heating/cooling procedures described in Section 2 were implemented.

To investigate further the thermal behavior of NPoGS, the procedure shown in Fig. 2 was developed. Following cooling at 10 C°/min, complex thermotropic behavior is again observed with transitions at 35°C, 39°C, and 53°C (heating rate, 5 C°/min; Fig. 2a); note however that prior cooling rate affects the relative enthalpy of transitions I and II (c.f. Fig. 1a and Fig. 2a). NPoGS cooled at 10 C°/min shows the cooling exotherm to be at −2°C at this

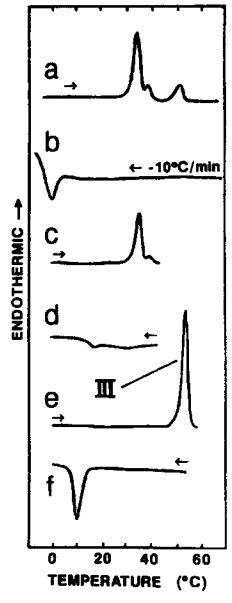

Fig. 2. DSC behavior of NPoGS (all scans, except (b), are at 5 C°/min): (a) Initial heating scan immediately following cooling from 70°C at 10 C°/min, (b) Cooling scan at 10 C°/min, (c) Heating scan to 46°C, between transitions II and III, (d) Immediate cooling scan, (e) Immediate heating scan to 60°C, (f) Cooling scan.

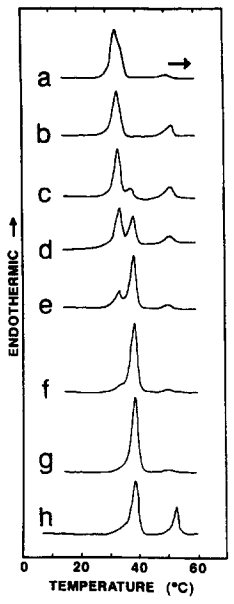

Fig. 3. DSC heating curves of NPoGS recorded at 5 C°/min immediately following cooling at different rates of (a) 40, (b) 20, (c), 10, (d) 5, (e) 2.5, (f) 1.25, (g) 0.625 and (h) 0.3125 C°/min.

cooling rate (Fig. 2b). NPoGS was then heated above transitions I and II to 46°C (Fig. 2c). Immediate cooling to 0°C at 5 C°/min shows a significant reduction in the enthalpy of the cooling exotherm (Fig. 2d) compared to those shown in Fig. 1b and Fig. 2b. The subsequent heating curve (Fig. 2e) shows no evidence of transitions I (35°C) and II (39°C), and resulted in a marked increase in the enthalpy of transition III (53°C) from ~ 1 kcal/mol (Fig. 1a or Fig. 2a) to 12 kcal/mol (Fig. 2e). The subsequent cooling scan at 5 C°/min (Fig. 2f), again produced an exotherm at 10°C similar to that shown in Fig. 1b but lacking the high temperature shoulder. Thus, NPoGS could be converted completely into the phase (phase III) responsible for transition III (Fig. 2e) by a heating/cooling cycle through transitions I and II.

To isolate the phases responsible for transitions I and II, the following protocol was used. Varying the cooling rates between 0.3125 C°/min and 40 C°/min prior to immediate heating at 5 C°/min results in the DSC scans displayed in Fig. 3. Prior cooling faster than 10 C°/min (Fig. 3a and b) favors the formation of the phase which produces transition I ($T = 32$°C). Cooling at rates between 2.5 C°/min and 10 C°/min (Fig. 3c–e) reproduces the complex DSC behavior shown previously (see Fig. 1a and Fig. 2a) with all three transitions apparent. Cooling at rates slower than 2.5 C°/min (Fig. 3f and g) favors the phase which produces transition II, whereas cooling at the slowest rate (0.3125 C°/min, Fig. 3h) leads to a conversion of NPoGS into the phases which give rise to transitions II and III. Although more pronounced at certain scanning rates, transition III is observed in the DSC heating curves immediately following all prior cooling scan rates. However, it

is clear that manipulation of the prior cooling rate can be used to isolate in a quite pure form the phases giving rise to peaks I (prior cooling rate 40 C°/min) and II (prior cooling rate, 0.625 C°/min)..

To obtain the true molar enthalpies of transitions I and II, correction for the presence of minor amounts of NPoGS in phase III is required (see Fig. 3b and g). Since the enthalpy of transition III alone had been determined, ΔH_{III} = 12.8 kcal/mol (Fig. 4A), the molar amount of NPoGS in phase III present in the DSC heating scans shown in Fig. 3b and g could be determined, and a correction factor introduced for the enthalpy calculations for transitions I and II. Analysis of transition I, as produced by a pre-scan cooling rate of 20 C°/min (Fig. 3b) and corrected for the presence of the phase giving rise to transition III, resulted in a transition enthalpy ΔH_I = 6.3 kcal/mol; transition II, as produced by a pre-scan cooling rate of 0.625 C°/min (Fig. 3g) and corrected in a similar fashion, gave ΔH_{II} = 8.6 kcal/mol.

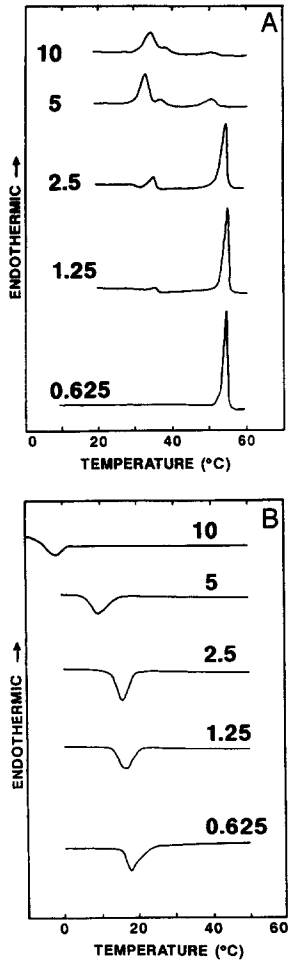

Fig. 4. DSC heating/cooling curves of NPoGS as a function of scan rate: (A) DSC heating curves. Scan rates (C°/min) are listed to the left of their respective heating curves. All heating scans were performed after samples were cooled from 70°C at 10 C°/min. (B) DSC cooling curves. Scan rates are listed to the right of their respective cooling curves. All scans were executed after samples were heated to 70°C at 5 C°/min.

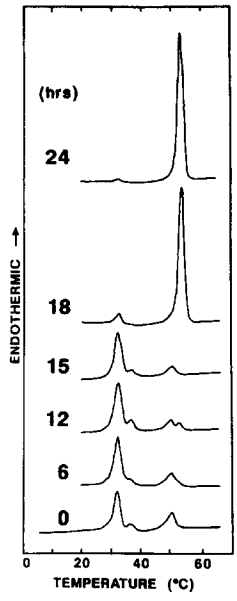

Fig. 5. DSC heating curves of NPoGS following incubation at −12°C. Incubation time in hours is listed to the left of its respective heating curve. All samples were cooled at 10 C°/min from 70°C before incubation. All heating curves shown were scanned at 5 C°/min.

Fig. 4A shows the effect of varying the heating rate after NPoGS has been cooled from 70°C at 10 C°/min. Fig. 4B shows the subsequent cooling scans immediately recorded at different cooling rates. Heating at 10 C°/min results in DSC behavior similar to the reversible behavior seen in Fig. 2a and Fig. 3c; there is a complex transition (I and II) with maxima at 35°C and 39°C, and a high temperature transition (III) at 53°C. As the heating rate is decreased the enthalpies of transitions I and II decrease, whereas the enthalpy of transition III increases until, at a heating rate of 0.625 C°/min, transitions I and II are no longer observed. Correspondingly, the enthalpy of peak III at 53°C increases, reaching a limiting value ΔH = 12.8 kcal/mol at 0.625 C°/min. All the subsequent cooling scans yielded a single exotherm with ΔH = 5 kcal/mol (Fig. 4B). At the faster cooling rates, there is clear evidence of supercooling; as the cooling scan rate was decreased from 10 C°/min to 0.625 C°/min, the transition temperature increased from −3°C to a limiting value of 17°C. Even at the slowest heating and cooling rates (0.625 C°/min) there is clear evidence of hysteresis with the transition on heating occurring at 51°C and that on cooling at 17°C (Fig. 4A and B).

Incubating NPoGS at low temperatures also favored the formation of the phase giving rise to transition III. The effect of incubating NPoGS at −12°C is presented in Fig. 5. Before incubation, NPoGS was cooled at 10 C°/min to −12°C. Immediate reheating at 5 C°/min shows similar behavior to that described previously (see, for example, Fig. 2a, Fig. 3c and Fig. 4) with transitions at 35, 39, and 51°C; similar behavior is observed after 6 h incubation. Following low temperature incubation for 12 h, the high

temperature transition became complex with maxima at both 51°C and 53°C, but without significant increase in enthalpy. The behavior was not readily reproducible as the heating scan following a 15 h incubation shows only a single peak at 51°C. Although there does appear to be some variability associated with transition III, we have not been able to probe the structural basis for this variability. With further increase in incubation time (see 18 and 24 h incubations), transitions I and II decrease markedly in enthalpy with a corresponding large increase in transition enthalpy for transition III at 53°C (c.f. higher temperature transition at 12 h incubation). For incubation times of 24 h or greater, further decreases in the enthalpy of transitions I and II are accompanied by an increase in the enthalpy of transition III. The low temperature transitions virtually disappear (Fig. 5), and the enthalpy of transition III reaches its maximum value, $\Delta H = 12.8$ kcal/mol.

Finally, to investigate the cooling behavior immediately following the three individual transitions I, II, and III, protocols were implemented which gave rise to essentially single transitions I, II, and III on heating; then, immediately, a cooling scan was recorded at 5 C°/min. To obtain transition I, NPoGS was cooled from 70°C at 10 C°/min prior to heating at 5 C°/min (Fig. 6A, top); transition II was observed following cooling from 70°C at 0.625 C°/min and heating at 5 C°/min (Fig. 6B, top); and transition III was observed by heating NPoGS at 0.625 C°/min (Fig. 6C, top). The cooling scans (at 5 C°/min) following each of these procedures are presented in the lower curves of Fig. 6A–C. Transition temperatures and enthalpies from the cooling scans produced after melting

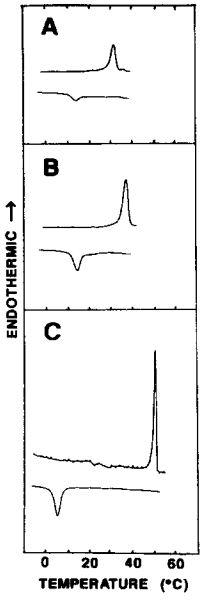

Fig. 6. DSC heating/cooling curves after isolating each of the three low temperature phases; (A) L_I, (B) L_{II}, and (C) L_{III}. Heating rates: 5 C°/min, 5 C°/min, 0.625 C°/min, respectively; cooling rates: all 5 C°/min.

phases giving transitions I, II and III are as follows: 14°C,. 0.8 kcal/mol; 14°C, 3.2 kcal/mol; and 5°C, 5.4 kcal/mol, respectively. Clearly, in all cases the enthalpy observed for the cooling transitions is significantly less than that observed on heating, again indicating the hysteresis and slow kinetics of the cooling transitions.

Based on the DSC procedures reported above, X-ray diffraction patterns were collected for the phases of NPoGS responsible for transitions I, II, and III.

3.2. X-ray diffraction

X-ray diffraction patterns of fully hydrated NPoGS recorded at −12°C and 0°C immediately following initial equilibration at 70°C (see Section 2) were complex, reflecting the presence of multiple phases. To eliminate the complexity in the diffraction patterns, heating and cooling protocols which gave rise to single phases as observed by DSC (see above) were performed on samples prior to the recording of the X-ray diffraction patterns.

Phase I, the phase which gives rise to transition I, was isolated by rapidly cooling NPoGS from 70°C to 0°C at rates greater than 20 C°/min by quenching NPoGS samples in an ice/water bath. The X-ray diffraction pattern produced by phase I, recorded immediately at 0°C, is presented in Fig. 7A. This diffraction pattern has low angle reflections of orders $h = 1$ to 10, corresponding to a lamellar periodicity, d, of 50.7 Å; a strong wide angle reflection is present at 4.1 Å, characteristic of a bilayer gel phase with hexagonal chain packing (L_I).

The X-ray diffraction pattern of phase II resulting from slowly cooled NPoGS (scan rate = 1 C°/min, from 70°C to 0°C), the procedure giving transition II by DSC, is shown in Fig. 7B. Recorded immediately at 0°C, this pattern has lamellar low angle reflections $h = 1$ to 10, $d = 51.7$ Å, and strong wide reflections at 4.9, 4.6, 4.2, and 4.0 Å, as well as weaker reflections at 5.1 and 3.8 Å, implicating phase II as a bilayer phase (L_{II}) with more ordered chain packing than that of phase I.

Heating NPoGS at 1 C°/min from −12°C to 46°C, and recording at 46°C, gives the X-ray diffraction pattern corresponding to phase III (Fig. 7C). This X-ray diffraction pattern shows low angle reflections $h = 1$ to 6, $d =$ 49.2 Å, and strong wide angle reflections at 4.6 Å and 4.2 Å identifying phase III as a bilayer phase with ordered chain packing (L_{III}).

At temperatures above that of transition III the X-ray diffraction pattern shown in Fig. 7D is obtained. This diffraction pattern shows a lamellar periodicity of $d = 49.2$ Å from low angle reflections $h = 1$ to 4 and a diffuse wide angle reflection at 4.5 Å, clearly indicating a melted-chain L_α bilayer phase.

Finally, X-ray diffraction patterns were recorded at higher temperatures immediately after recording the X-ray diffraction patterns for the three individual low tempera-

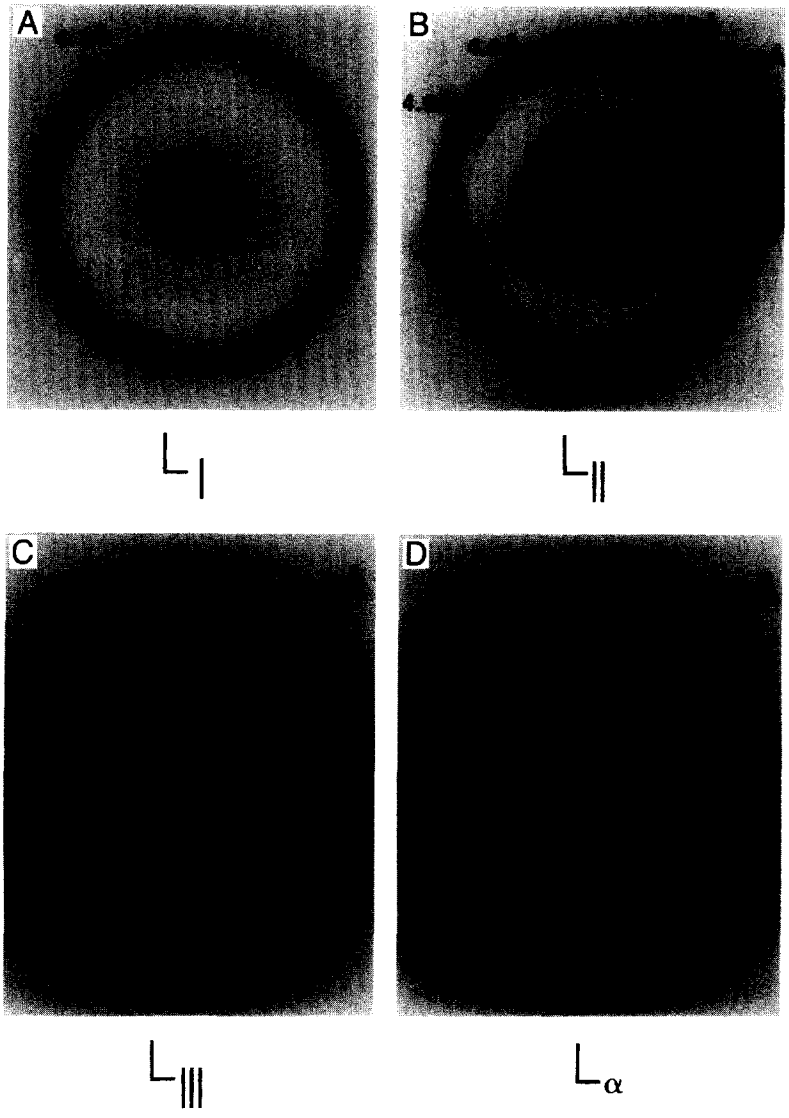

Fig. 7. X-ray diffraction patterns of NPoGS: (A) L_I at 0°C, (B) L_{II} at 0°C, (C) L_{III} at 46°C, (D) L_α at 60°C.

ture phases. The diffraction pattern was collected at temperatures above the respective transition temperatures of each low temperature phase: 38°C for phase I; 46°C for phase II, and 65°C for phase III (data not shown). All three X-ray diffraction patterns corresponded to that of an L_α phase indicating a direct transition from each low temperature phase to the melted-chain L_α phase. For the diffraction patterns recorded at 38°C and 46°C there was no evidence of conversion of NPoGS to phase III during the time course ($\sim$ 6 h) of the experiment, a single bilayer phase with multiple low angle reflections indexing to a unique bilayer periodicity being observed in each case.

4. Discussion

The complex behavior exhibited by fully hydrated NPoGS in Fig. 1 leads to a question of its origin. It is obvious that three low temperature phases exist, but whether one gives rise to another serially, via polymorphic transformation, or whether multiple phases are produced on cooling and combinations of phases coexist was unclear. The results of the DSC experiments shown in Figs. 2–5 provide strong evidence that the latter hypothesis is correct. If these phases occurred as a result of serial polymorphic transformations (i.e., if phase L_I gave rise to phase L_{II}, which gave rise to phase L_{III}, on heating, L_I should always be followed by L_{II}, and L_{II} should always be followed by L_{III}). This is clearly not the case. As shown in Fig. 3, the prior cooling rate significantly influences the thermotropic behavior observed on subsequent heating. Further evidence is provided by the X-ray diffraction data. The X-ray diffraction patterns taken at temperatures above the transition temperatures of all three individual low temperature phases at 38°C, 46°C, and 65°C, show *only* the melted-chain L_α phase, thus indicating a direct

transformation of NPoGS from any of its low temperature phases to the melted-chain L_α phase. There is no evidence of $L_I \rightarrow L_{II} \rightarrow L_{III}$ polymorphic transformations.

Phase L_{III} has the highest transition temperature and enthalpy, identifying it as the most stable phase. The DSC results illustrated in Fig. 4A and Fig. 5 reflect this. Fig. 4A shows a shift to L_{III} as the predominant phase upon decrease in the heating rate and Fig. 5 shows a conversion to L_{III} upon low temperature incubation. Thus, slow heating or low temperature incubation favor the production of L_{III} over L_I and L_{II}. An interesting aspect of the conversion to L_{III} upon low temperature incubation is that it happens quite rapidly (Fig. 5), with a large change in the relative enthalpy of transition III to those of transitions I and II occurring between 15 and 18 h. This suggests that an isothermal conversion from L_I and/or L_{II} to L_{III} at low temperatures occurs through a slow nucleation-fast growth event, although other factors including steric/conformational constraints may certainly be involved.

When NPoGS was incubated for long times at temperatures below that of transition III (e.g., 38°C and 45°C), the X-ray diffraction patterns were complex, but consistently showed the presence of L_{III}. Although it may be kinetically slow, NPoGS will convert to L_{III} at any temperature below the L_{III} transition temperature. Further evidence can be seen in the DSC data presented in Fig. 5 (incubation at −12°C) and in DSC data recorded following incubation at 38°C and 45°C (data not shown). These DSC scans all showed an increase in the enthalpy of transition III with increased incubation time at all temperatures (−12°C, 38°C, and 45°C).

The behavior of NPoGS on cooling is illustrated in Fig. 4B and Fig. 6. In contrast to the complex thermotropic behavior observed on heating, cooling from the melted-chain L_α phase shows only a single, albeit broad, transition. As shown in Fig. 6, there does appear to be a decrease in the recrystallization temperature following melting of the L_{III} phase. The X-ray diffraction data argue that the L_α phases formed are independent of the phase (L_I, L_{II} or L_{III}) from which they are formed. Presumably the different levels of supercooling and the differences in enthalpy observed for the cooling exotherm are additional manifestations of the complex phase behavior of NPoGS, notably the availability of multiple 'ordered chain' phases on recrystallization. As the cooling rate is increased,

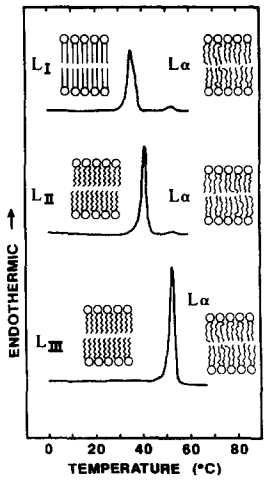

Fig. 8. Summary of the thermotropic and structural behavior of the isolated L_I, L_{II} and L_{III} phases of hydrated NPoGS. Circles represent the galactose head groups; zigzag tail, crystalline chain; straight (line) tail, ordered/gel chain; wiggled tail, melted chain. DSC heating curves for the L_I, L_{II} and L_{III} phases are also shown.

NPoGS exhibits a degree of supercooling, as illustrated in Fig. 4B. The speculation that NPoGS depends upon seed crystals for nucleation of the L_{III} phase is supported by the DSC scans following low temperature incubation (Fig. 5), and by X-ray diffraction patterns taken at low temperatures after heating and cooling NPoGS below 45°C. The DSC data indicated a clear preference for formation of the L_{III} phase, possibly due to unmelted L_{III} acting as seed crystals. However, despite the large endothermic enthalpy associated with transition III (12.8 kcal/mol), the exothermic enthalpy on cooling was always less than 6 kcal/mol. Even when seed crystals are present, NPoGS may exhibit only limited conversion to the L_{III} phase on cooling and the other low temperature phases L_I and L_{II} may form.

The thermotropic and structural behavior of NPoGS are summarized in Fig. 8 and Table 1. The X-ray diffraction data show that NPoGS exhibits three low temperature bilayer phases with gel/crystalline chain packing, which we have called L_I, L_{II}, and L_{III}. Each of these three phases converts directly into L_α when heated at 5 C°/min. L_I is the least ordered of the low temperature phases ($L_I \rightarrow L_\alpha$ transition entropy, $\Delta S_I = 20.6$ e.u.), is metastable, and is formed when NPoGS is rapidly cooled; L_{II} has a degree of order ($L_{II} \rightarrow L_\alpha$, $\Delta S_{II} = 27.6$ e.u.) intermediate between those of L_I and L_{III}, an ordered,

Table 1
Thermodynamic and structural parameters of NPoGS

Phase	Transition		Lamellar periodicity (Å)	Wide angle reflections (Å)
	temp. (°C)	ΔH (kcal/mol)		
L_I	35	6.3	50.7	4.1
L_{II}	39	8.6	51.7	3.8/4.0/4.2/4.6/4.9/5.1
L_{III}	53	12.8	49.2	4.2/4.6
L_α			49.2	4.5

Table 2
Thermodynamic parameters of galactosyl cerebrosides

Galactosyl cerebroside *N*-linked acyl chain	Transition	Temp. (°C)	ΔH (kcal/mol)	ΔS (e.u.)
16:0	HT	82	17.5	49.3
16:1	I	35	6.3	20.6
	II	39	8.6	27.6
	III	53	12.8	39.2
18:0	HT	85	18.0	50.3
18:1	MS	45	11.5	36.1
	HT	55.5	12.1	36.8
18:2	MS	28	8.0	26.6
	HT	44	9.8	30.9
24:0		82	15.3	43.1

MS, metastable phase.
HT, high temperature, most stable phase.

crystalline chain packing mode as indicated by the wide angle X-ray diffraction data, and is formed when NPoGS is cooled at intermediate rates; and L_{III} is the most ordered ($L_{III} \rightarrow L_{\alpha}$, $\Delta S_{III} = 39.2$ e.u.), is the stable low temperature form of NPoGS with ordered, crystalline chain packing, and is formed when NPoGS is slowly cooled or incubated at temperatures below 50°C.

In some cases it is possible to use the pattern of the strong wide angle reflections to determine the hydrocarbon packing in terms of one of the simple chain packing subcells, e.g., triclinic, orthorhombic, monoclinic, etc. [31,32]. However, it has been shown that more complex chain-packing modes are adopted by phospholipids and glycolipids and a direct interpretation of the wide angle reflections in terms of a specific chain packing mode is not possible [33,34]. For NPoGS, L_I appears to be a gel phase with rotationally-disordered, hexagonally-packed chains, whereas both L_{II} and L_{III} adopt more specific, but as yet undefined, crystalline chain packing modes. The small changes in bilayer periodicity observed when L_I, L_{II} and L_{III} undergo chain-melting to L_{α} (Table 1) are presumably due to offsetting changes in chain tilt/conformation and hydration affecting the bilayer and hydration layer thicknesses, respectively.

In the past, we have studied fatty acyl chain variations of a series of cerebrosides, which included the *N*-linked 16:0, 18:0, 18:1, 18:2 and 24:0 galactosyl cerebrosides [13–15]. The pertinent thermodynamic data from these papers are summarized in Table 2. Ruocco et al. [13] demonstrated that hydrated 16:0 cerebroside converted between metastable and stable bilayer structures with the stable form exhibiting a high temperature/high enthalpy (82°C, 17.5 kcal/mol) chain-melting transition; the metastable form is similar to anhydrous crystalline 16:0 cerebroside, which is converted to the stable form on hydration.

Reed and Shipley [15] elucidated the thermotropic behavior of 18:0, 18:1, and 18:2 galactosyl cerebrosides. All three of these cerebrosides assume multiple low temperature phases. Upon heating at 5 C°/min, 18:0 cerebroside displays a reversible high temperature/high enthalpy endotherm and an irreversible exotherm produced by a metastable phase, behavior similar to that of the 16:0 cerebroside [13,15]. The 18:1 and 18:2 cerebrosides each have a metastable low temperature form and a stable form. The stable forms give rise to high temperature/high enthalpy endothermic transitions. For 18:0, 18:1, and 18:2 galactosyl cerebrosides, the high temperature/high enthalpy transitions are at 85°C, 55.5°C, and 44°C, and have enthalpies of 18:0 kcal/mol, 12.1 kcal/mol, and 9.8 kcal/mol, respectively. The metastable forms of 18:1 and 18:2 cerebrosides undergo endothermic transitions at 45°C and 28°C with enthalpies of 11.5 kcal/mol and 8.0 kcal/mol, respectively. X-ray diffraction studies showed all the low temperature forms to be bilayers with different types of crystalline chain packing. 24:0 galactosyl cerebroside also exhibits metastable and stable forms, the latter undergoing a high enthalpy transition at 82°C [14].

The effects of chain length and unsaturation for this series of galactosyl cerebrosides can now be compared. For saturated chain cerebrosides, an increase in chain length of the *N*-linked fatty acid from 16:0 to 18:0 increases the transition temperature of the most stable phase; however, 24:0 cerebroside undergoes chain-melting of the stable phase at a lower temperature (82°C). An increase in unsaturation at a constant chain length always decreases the transition temperature (and enthalpy and entropy) of the most stable phase (Table 2). The most stable phase of NPoGS has a significantly lower transition temperature and enthalpy than that of the saturated chain 16:0 cerebroside and a slightly lower transition temperature (but similar enthalpy) than that of the longer chain unsaturated 18:1 galactosyl ceramide.

Finally, we consider the kinetics of the transitions of NPoGS compared to those of other cerebrosides. Fully hydrated 16:0 and 18:0 galactosyl cerebrosides show a transition exotherm below the transition temperature of the most stable phase, the exotherm representing a conversion of the metastable phase to the most stable form. This is not the case with the unsaturated fatty acid 16:1, 18:1, and 18:2 cerebrosides. The metastable forms of the 16:1, 18:1, and 18:2 cerebrosides are stable enough to prevent their *direct* conversion to their most stable phases through an exothermic event, at least as observed at heating rates of 5 C°/min. Thus, an interesting kinetic dimension is highlighted by the comparative behavior of cerebrosides; the introduction of any unsaturation in the *N*-linked fatty acyl chains inhibits direct conversion to and formation of the most stable phase from the less stable phases.

Acknowledgements

We thank Dr. Robert A. Reed for his helpful advice and thoughtful criticisms. We thank Irene Miller for help with

the preparation of the manuscript. This work was supported by National Institutes of Health research grant HL-26335 and training grant HL-07291.

References

[1] Linington, C. and Rumsby, M.G. (1978) Adv. Exp. Med. Biol. 100, 263–273.
[2] Rumsby, M.G. (1978) Biochem. Soc. Trans. 6, 448–462.
[3] Bunow, M.R. and Levin, I.W. (1980) Biophys. J. 32, 1007–1022.
[4] Skarjune, R.P. and Oldfield, E. (1979) Biochim. Biophys. Acta 556, 208–218.
[5] Huang, T.H., Skarjune, R.P., Wittebort, R.J., Griffin, R.G. and Oldfield, E. (1980) J. Amer. Chem. Soc. 102, 7377–7379.
[6] Lee, D.C., Miller, I.R. and Chapman, D. (1986) Biochim. Biophys. Acta 859, 266–270.
[7] Clowes, A.W., Cherry, R.J. and Chapman, D. (1971) Biochim. Biophys. Acta 249, 301–317.
[8] Bunow, M.R. (1979) Biochim. Biophys. Acta 574, 542–546.
[9] Freire, E., Bach, D., Correa-Freire, M., Miller, I. and Barenholz, Y. (1980) Biochemistry 19, 3662–3665.
[10] Linington, C. and Rumsby, M.G. (1981) Neurochem. Int. 3, 211–218.
[11] Curatolo, W. (1982) Biochemistry 21, 1761–1764.
[12] Curatolo, W. and Jungawala, F.B. (1985) Biochemistry 24, 6608–6613.
[13] Ruocco, M.J., Atkinson, D., Small, D.M., Skarjune, R.P., Oldfield, E. and Shipley, G.G. (1981) Biochemistry 20, 5957–5966.
[14] Reed R.A. and Shipley, G.G. (1987) Biochim. Biophys. Acta 896, 153–164.
[15] Reed, R.A. and Shipley, G.G. (1989) Biophys. J. 55, 281–292.
[16] Maggio, B., Cumar, F.A. and Caputto, R. (1981) Biochim. Biophys. Acta 650, 69–87.
[17] Maggio, B., Cumar, F.A. and Caputto, R. (1978) Biochem. J. 175, 1113–1118.
[18] Maggio, B., Cumar, F.A. and Caputto, R. (1978) Biochem. J. 171, 559–565.
[19] Reiss-Husson, F. (1967) J. Mol. Biol. 25, 363–382.
[20] Abrahamsson, S., Pascher, I., Larsson, K. and Karlsson, K.-A. (1972) Chem. Phys. Lipids 8, 152–179.
[21] Fernandez-Bermudez, S., Loboda-Cackovic, J., Cackovic, H. and Hosemann, R. (1977) Z. Naturforsch. 32, 362–374.
[22] Hosemann, R., Loboda-Cackovic, J., Cackovic, H., Fernandez-Bermudez, S. and Balta-Calleja, F.J. (1979) Z. Naturforsch. 34C, 1121–1124.
[23] Pascher, I. and Sundell, S. (1977) Chem. Phys. Lipids 20, 175–191.
[24] Coolbear, K.P., Berde, C.B. and Keough, K.M.W. (1983) Biochemistry 22, 1466–1472.
[25] Skarjune, R.P. and Oldfield, E. (1982) Biochemistry 21, 3154–3160.
[26] Radin, N.S. (1976) J. Lipid Res. 17, 290–293.
[27] Radin, N.S. (1974) Lipids 9, 358–360.
[28] Radin, N.S. (1972) Methods Enzymol. 28, 300–306.
[29] Elliott, A.J. (1965) J. Sci. Instrum. 42, 312–316.
[30] Franks, A. (1958) Brit. J. Appl. Phys. 9, 349–352.
[31] Maulik, P.R., Ruocco, M.J. and Shipley, G.G. (1990) Chem. Phys. Lipids 56, 123–133.
[32] Abrahamsson, S., Stallberg-Stenhagen, S. and Stenhagen, E. (1963) Prog. Chem. Fats Other Lipids 7, 59–96.
[33] Abrahamsson, S., Dahlen, B., Lofgren, H. and Pascher, I. (1978) Prog. Chem. Fats Other Lipids 16, 125–143.
[34] Shipley, G.G. (1986) in The Physical Chemistry of Lipids From Alkanes to Phospholipids (Small, D.M., ed.), pp. 97–147, Plenum Press, London.